.

–

MODELING SCRAMJET SUPERSONIC COMBUSTION VIA EDDY DISSIPATION MODEL

Jimmy-John O.E. Hoste [a*] **, Marco Fossati** [b]
Laboratory for Future Air-Space Transportation Technology
University of Strathclyde, United Kingdom

Ian J. Taylor [c]
Division of Aerospace Sciences
University of Glasgow, United Kingdom

Rowan J. Gollan [d]
Centre for Hypersonics
University of Queensland, Australia

Scramjet technology has gained considerable interest in multi-stage to orbit design concepts due to its reusability and high specific impulse at high-Mach regimes. The aim of the present work is to introduce Reynolds Averaged Navier-Stokes CFD calculations in the design phase of scramjet vehicles and increase the fidelity of engine performance assessment. The turbulence-chemistry interaction is described by the Eddy Dissipation Model (EDM) introduced by Magnussen and Hjertager, which assumes that turbulent motions and not chemistry is the main driver in the rate of combustion. The use of the EDM is explored by application to three hydrogen–fueled scramjet test cases. The model requires constants to be prescribed, which are found to be case dependent. Optimal values for the cases simulated are discussed along with appropriateness of the model for general design simulations. The advantage in computational cost is demonstrated by comparison with a no-model finite-rate chemistry approach.
Keywords: scramjet, k-ω 2006, Eddy Dissipation Model

1. Introduction

In the past decade the small satellite market has seen a considerable growth resulting in an increased demand for an economically viable, more reliable and flexible access to space. To address the demand, smaller rocket launchers with limited payload capacity are being introduced. In the context of small launchers, scramjet technology could be a viable option given its reusable character, higher specific impulse at high-Mach regime as well as increased safety and reliability. The Australian SPARTAN program aims at exploring the advantages of scramjets by designing a three-stage-to-orbit rocket-scramjet-rocket launch system with reusable first and second stages [1, 2].

Designs incorporating scramjet engines typically rely on one- or quasi-one dimensional low-fidelity numerical tools for engine performance characterization in the form of a propulsion database [1, 2]. Details about specific impulse, mass flow rate of fuel / oxidizer and maximum possible equivalence ratio at multiple design points along a trajectory are contained in this database, for example. The authors aim to replace the low-fidelity tools by higher fidelity numerical tools through the use of Computational Fluid Dynamics (CFD) in the early design phase. Among the CFD approaches, Reynolds-Averaged Navier-Stokes (RANS) remains the commonly adopted tool for design purposes in hypersonic propulsion flow paths [3, 4]. Therefore, a RANS–based modeling approach is sought for achieving the authors' aim. Within the RANS framework for scramjet propulsion, modeling turbulent combustion is one of the most challenging areas. In general, the approaches to describe turbulence chemistry interaction (TCI) are very demanding in terms of the computational cost and not demonstrably better for prediction in a general sense [3], therefore they are not the most effective option for design purposes. A more simplified way of looking at TCI could be considered for scramjet operation at high Mach regimes. At these Mach numbers, the combustion process takes place at very high speeds and is believed to be primarily limited by the rate at which air and fuel mix. Therefore, a TCI model is needed that takes into consideration the fact that turbulent mixing is the main driver of the rate of combustion. The Eddy Dissipation Model (EDM) introduced by Magnussen and Hjertager [5] appears to be an appropriate formulation for such type of TCI. Moreover, the EDM formulation is very advantageous

[a] PhD Candidate, jimmyjohn.hoste@strath.ac.uk
[b] Lecturer, marco.fossati@strath.ac.uk
[c] Senior Lecturer, ian.taylor@glasgow.ac.uk
[d] Lecturer, r.gollan@uq.edu.au
[*] Corresponding Author

in terms of computational cost as it alleviates the stiffness of the governing equations describing turbulent reacting flows [3] because only a reduced number of species that need to be tracked in the simulation, and there is only a single chemical timescale considered: the mixing–limited chemical timescale. Therefore, the present work will consider the effect of turbulence on combustion through the EDM.

The use of EDM in the modeling of scramjet flows has been reported in the literature by Edwards et al. [6] using the REACTMB in-house CFD solver as well as with commercial software by other authors [7, 8]. These studies demonstrate that EDM can be an adequate approach for design purposes. A recognized factor limiting the widespread adoption of EDM is the necessity of a fine calibration of the model parameters for which no consistent guidelines are available in the open literature for its optimal use on different scramjet configurations / operating conditions. The ongoing aim of the present work is to tackle such a limitation by assessing the predictive capability of the EDM for different types of hydrogen-fueled scramjets with a view to formulating general guidelines on the use of the model for scramjet analysis. In the first section, the governing equations for turbulent reacting flows are presented as well as the detailed formulation of the EDM. The following section describes the scramjet test cases used in this work followed by the results of the simulations. Finally, conclusions on the model are drawn based on the observations of the numerical predictions.

2. Numerical Modeling

The governing equations for turbulent compressible reacting flows can be written as
Mass Conservation:

$$\frac{\partial \bar{\rho}}{\partial t} + \frac{\partial}{\partial x_i}\left(\bar{\rho}\tilde{u}_i\right) = 0 \qquad [1]$$

Momentum Conservation:

$$\frac{\partial}{\partial t}\left(\bar{\rho}\tilde{u}_i\right) + \frac{\partial}{\partial x_j}\left(\bar{\rho}\tilde{u}_j\tilde{u}_i + \delta_{ij}\bar{p}\right) = \frac{\partial}{\partial x_j}\left(\bar{\tau}_{ji} - \widetilde{\bar{\rho}u_i'' u_j''}\right) \qquad [2]$$

Energy Conservation:

$$\frac{\partial}{\partial t}\left(\bar{\rho}\tilde{E}\right) + \frac{\partial}{\partial x_j}\left(\bar{\rho}\tilde{u}_j\tilde{H}\right) = \frac{\partial}{\partial x_j}\left(\bar{\tau}_{ij}\tilde{u}_i + \overline{\tau_{ij}u_i''} - \bar{q}_j - \widetilde{\bar{\rho}H'' u_j''}\right) \qquad [3]$$

Species Conservation:

$$\frac{\partial(\bar{\rho}\tilde{Y}_s)}{\partial t} + \frac{\partial(\bar{\rho}\tilde{Y}_s\tilde{u}_j)}{\partial x_j} = \bar{\dot{\omega}}_s - \frac{\partial}{\partial x_j}\left(\bar{J}_{s_j} + \widetilde{\bar{\rho}Y_s'' u_j''}\right) \qquad [4]$$

with conserved variables $\bar{\rho}$, $\bar{\rho}\tilde{u}_j$, $\bar{\rho}\tilde{E}$, $\bar{\rho}\tilde{Y}_s$ representing in order of appearance density, momentum, total energy per unit volume and partial densities of the species s (s=1,. . .,N). Throughout this work, the above set of equations will be referred to as the Reynolds Averaged Navier-Stokes equations (RANS). The symbols $\bar{x}$ and $\tilde{x}$ denote respectively the time and Favre (or density-weighted) average. Equations 1 to 4 are written in such a way that those terms which require modeling are indicated on the right-hand side. The system of conservation equations for a turbulent chemically reacting flow needs extensive modeling. A comprehensive overview of the modeling practice for supersonic internal flows can be found in the work of Baurle [3]. The present work will only address the treatment of the mean species reaction rates $\bar{\dot{\omega}}_s$.

In this work, the RANS equations are solved with the Eilmer [b] [9, 10] open-source CFD package, developed at the University of Queensland. The finite volume solver addresses turbulence closure by means of Wilcox's 2006 $k-\omega$ model [11] and has been previously validated for scramjet type flows [12, 13]. Shock capturing is ensured by treating the inviscid fluxes with an adaptive method switching between Macrossan's Equilibrium Flux Method (EFM) [14] and Liou and Wada's AUSMDV [15]. With its more diffusive character, the former is active in regions with strong gradients in Mach while the latter is used elsewhere. Viscous fluxes are treated by means of Gauss' theorem and the forward Euler scheme is used for the time integration. The main modeling issue in high-speed reacting flows is the chemical source term $\bar{\dot{\omega}}_s$ which is highly non-linear and cannot be directly related to mean flow properties. Turbulence can considerably affect the combustion process by either promoting or suppressing reactions. It is the role of the TCI model to describe this effect through the chemical source term. In scramjet flow studies, the use of the "no-model" or Arrhenius approach is commonly adopted where the law of mass action is applied for a given reaction mechanism. TCI is completely ignored and could be acceptable when chemical time scales are larger than flow time scales [16]. Examples of supersonic combustion modeling with RANS and the no-model approach, for hydrogen as fuel, can be

[b] http://cfcfd.mechmining.uq.edu.au/eilmer

found in the literature for the experiments of Burrows-Kurkov [17–23], SCHOLAR [24,25], JAXA's scramjet [26] and the HyShot [27–29]. Depending on the test case, the no-model choice did provide satisfactory results, however other studies demonstrated the need to include the effect of turbulence on the chemistry which, in most cases, increases the computational cost. Studies adopting a TCI model such as Probability Density Functions (PDF), a flamelet model or Eddy Dissipation Concept / Model can be found applied to the experiments of Burrows-Kurkov [30, 31], SCHOLAR [7], DLR [8,32–36] and the HyShot [29,37,38].

When RANS is applied in a design context, the use of sophisticated TCI models can be a disadvantage due to the increased computational requirements. Therefore this work seeks a model suitable for design while ensuring a certain degree of correctness in predictions inlcuding effects of turbulence on the chemistry. The Eddy Dissipation Model (EDM) introduced by Magnussen and Hjertager [5, 16] appears to be a good option. The idea of the model is the following: For fast chemical reactions fuel and oxidizer will react once they mix on a molecular scale. Assuming this fast chemistry limit, the rate at which reactions occur is then depedent on the rate at which turbulent eddies carrying fuel and oxidizer are brought together. In other words, the intermixing on a molecular level is dependent on the rate at which the eddies dissipate. From this description, the model can be also be referred to as "mixed-is-burned". The EDM is numerically implemented by assuming a single-step irreversible reaction of the form $\nu_F^{'} Fuel + \nu_O^{'} Oxidizer \rightarrow \nu_P^{''} Products$, where ν_s are the stoichiometric coefficients of Fuel (F), Oxidizer (O) and Products (P). Such a form is consistent with the model's physical description of fast-occurring chemical reactions. It must be noted that the model is limited to scramjet configuration where the chemical time scales are much smaller with respect to the turbulent time scales. The use of a single-step reaction instead of a reaction mechanism reduces the computational cost and makes it useful for design. In the case of hydrogen combustion, the reaction is : $2H_2 + O_2 \rightarrow 2H_2O$ and N_2 acting as an inert species resulting in four species equations (Equation 4). The reaction rate of fuel predicted by EDM is defined as:

$$\bar{\dot{\omega}}_F = -A_{edm}\ \bar{\rho}\beta^*\omega\ min\left[\tilde{Y}_F, \frac{\tilde{Y}_O}{s}, B_{edm}\frac{\tilde{Y}_P}{s+1}\right] \quad [5]$$

The oxidizer and product reaction rates can then be obtained as:

$$\bar{\dot{\omega}}_O = s\ \bar{\dot{\omega}}_F\ \ , \quad \bar{\dot{\omega}}_P = -(s+1)\bar{\dot{\omega}}_F \quad [6]$$

In the above equation s is the mass stoichiometric ratio defined as $s = (\nu_O^{'} W_O)/(\nu_F^{'} W_F)$ and equals 8 for H_2-air combustion. W_s is the molar mass in kg/mole and Y_s the mass fraction. In Equation 5, β^* is a turbulence model constant with a value of 0.09 and ω (1/s) is the specific dissipation of turbulent kinetic energy obtained through the turbulence model. The underlying physical assumption regarding the dissipation of turbulent eddies in the model is accounted for through the latter parameter. A_{edm} and B_{edm} are model constants which have standard values of 4.0 and 0.5. This combination of values follows from the work of Magnussen and Hjertager [5]. In the study of six different low-speed flame simulations, in conjunction with the k-ϵ turbulence model, satisfactory results in comparison with experimental data were obtained by adopting the above settings. In general, case dependent tuning of these parameters is required and is applied in this work. Edwards et al. [6] suggest a value for A_{edm} between 1 and 4. The mean fuel reaction rate of EDM, $\bar{\dot{\omega}}_F(kg/(m^3.s))$, is a function of turbulence (ω), and the mass fractions of fuel, oxidizer and products in every cell of the domain. Note that the latter term in the minimum evaluation of Equation 5 is intended to account for the effect of hot (or cold) products in a premixed turbulent flame situation where both fuel and oxidizer are contained within the same eddies [5]. The importance of the products on the combustion process can be controlled through the parameter B_{edm}. The premixed situation is not very common in scramjet flows except for the case of oxygen enrichment. Moreover, the inclusion of the product term implies that for reactions to occur an initial product mass fraction is required. This value is usually taken as 0.01. Unless otherwise stated, this work does not consider the product term.

EDM has a tendency to over-predict peak temperatures as well as the fuel consumption. The way to mitigate these disadvantages is by limiting $\bar{\dot{\omega}}_F$ with the reaction rate obtained with no-model approach and a single step global reaction [3]:

$$\bar{\dot{\omega}}_F = min(\bar{\dot{\omega}}_{F,edm}, \bar{\dot{\omega}}_{F,lam}) \quad [7]$$

where $\bar{\dot{\omega}}_{F,lam}$ is given by:

$$\bar{\dot{\omega}}_{F,lam} = -\nu_F^{'} W_F\ [k_f [X_F]^{\nu_F^{'}} [X_O]^{\nu_O^{'}} - k_r [X_P]^{\nu_P^{'}}] \quad [8]$$

The forward reaction rate k_f is obtained with Arrhenius law using a pre-exponential constant A=1.1e19 and an activation temperature T_A of 8052 K similar to Chandra Murty and Chakraborty [7]. These values have been obtained for hydrogen combustion by requiring that the flame speed of the single step kinetics match with those from full chemistry as pointed out by Sekar and Mukunda [39]. The backward or reverse reaction rate k_r is obtained from the forward rate and equilibrium constant. $[X_s]$ is the molar concentration. Another approach to reduce the over-predictions in fuel

consumption is by specifying an "ignition temperature" that has to be exceeded in every cell in order for combustion to occur. Edwards and Fulton [6] applied this for scramjet internal flow paths with a threshold of 900 K for hydrogen and ethylene. As pointed out by Baurle [3], the use of EDM does alleviate the stiffness of the governing equations as turbulent time scales are driving the reactions. In other words, sub-iterations coupled to chemical time scales are not required in order to reach the time step prescribed through the Courant-Friedrichs-Levy (CFL) criterion. This characteristic makes the use of EDM beneficial for design purposes.

In the case of non-premixed scramjet flow path simulations with EDM, on top of the model constant A_{edm}, values for turbulent Prandtl (Pr_t) and Schmidt number (Sc_t) have to be specified. Including the possibility to limit reaction rates with a threshold temperature (and /or the no-model reaction rate), this leaves the user to specify a combination of 4 (or 5) parameters per simulation. Details about the settings and effect of parameter values choices are presented in the following sections.

3. Test Cases

Three test cases are selected for study of the EDM on scramjet combustor flow fields. They are all characterized by different physical features which is suitable for assessing a model's predictive capability over a broad range of supersonic combustion phenomena. A first test case is the experiment of Burrows and Kurkov [40] with injection of hydrogen parallel to a vitiated airstream behind a backward facing step. The configuration enables the assessment of the EDM in a mixing layer environment. A second test case is the DLR combustor experiment of Waidmann et al. [41]. The geometry includes hydrogen injection behind a strut which is considered in certain scramjet designs. Two mixing layers are generated in this experiment adding complexity with respect to the experiment of Burrows and Kurkov. The last test case is the scramjet of Lorrain [42] relying on the concept of radical farming. The geometry differs from the two previous configurations as it does not allow for the development of mixing layers. Moreover, the design incorporates an intake and nozzle. In the first two test cases, a comparison with experimental data is presented, while for the third test case a comparison with CFD data is performed. Unity Lewis number is assumed throughout this work and in case of viscous walls the value of ω is set according to Menter's suggestion for smooth walls [43].

3.1 Case 1: Burrows-Kurkov

A commonly used test case in CFD code validation studies for supersonic combustion is the experiment of Burrows and Kurkov [40] (BK) shown in Figure 1. The popularity of the configuration follows from an extensive set of comparison data in pure mixing and reacting conditions. Many authors have performed RANS studies of the geometry without TCI over the last three decades with varying degrees of success. [17–23, 30, 44, 45] The test case is known to be very sensitive to the the values of turbulent Prandtl (Pr_t) and Schmidt (Sc_t) numbers. Following a sensitivity study for Wilcox k-ω 2006 model in Eilmer it was observed that the combinations $Pr_t = 0.9$, $Sc_t = 0.5$ and $Pr_t = 0.5$, $Sc_t = 0.5$ gave very similar results in comparison with the experimental data at the exit of the combustor in non-reacting conditions and with finite-rate chemistry. The results with the latter combination are presented in this work.

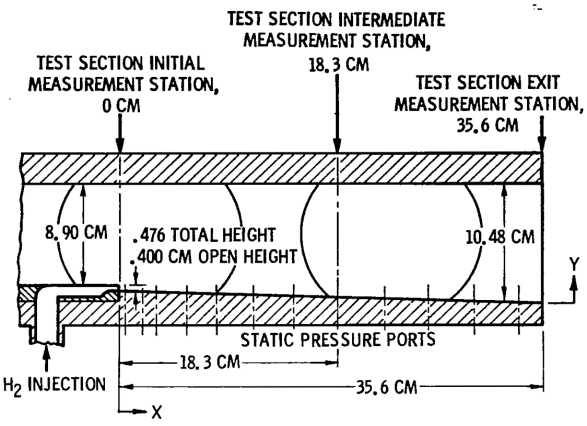

Fig. 1: Schematic of the Burrows-Kurkov supersonic combustion experiment [40].

3.1.1 Problem Formulation

The experimental setup in Figure 1 has been simulated in two stages. In the first stage, a boundary layer section (BLS) of 65 cm is considered using the same vitiated air supersonic inflow conditions as Edwards et al. [46] listed in Table 1. Note that these values differ from the ones typically encountered in the literature, however Edwards et al. [46] demonstrated a very good agreement overall with experiments in their work. Values for turbulence intensity (I) and the ratio of turbulent to laminar viscosity (μ_t/μ) are set to 5 % and 10 respectively. The exit profile of the first stage is used as an inflow condition for the second stage which considered the geometry depicted in Figure 1 with a BLS of 2 cm. The injector is simulated as a constant area channel of 2.2 cm with conditions in Table 1. Turbulence boundary conditions for the injector are the same as for the separate BLS simulations. Walls are treated isothermal at a temperature of 300 K and a supersonic outflow is prescribed where values from the interior of the domain are extrapolated. The

structured grid for the second stage contained 185 920 cells and the maximum first cell distance to physical walls was below 5e-6 m ensuring that the first cell is in the viscous sublayer.

Table 1: Inflow and injector flow conditions for Burrow-Kurkov' experiment.

	inflow	injector
u (m/s)	1741.4	1217.0
T (K)	1237.9	254.0
p (Pa)	96000.0	101350.0
Y_{H_2} (-)	0.0	1.0
Y_{O_2} (-)	0.258	0.0
Y_{H_2O} (-)	0.256	0.0
Y_{N_2} (-)	0.486	0.0

3.1.2 Results

Figures 2 and 3 show respectively the composition (mole fraction) and total temperature at the exit of the geometry (x=35.6cm in Figure 1) obtained with different settings of the EDM constant (A_{edm}) as well as with the no-model approach. The latter has been simulated with the 7 species, 8 reactions mechanism of Evans-Schexnayder (E-S) with modified third-body efficiencies in accordance with Bhagwandin et al. [21] The horizontal axis represents the distance from the lower wall. Results with E-S are very similar to what Bhagwandin et al. [21] reported with the k-ω Shear Stress Transport (SST) model and follow the experimental trend (symbols). Simulations with the use of the EDM have not been limited with the no-model global reaction or a threshold temperature in the Figures. In a separate study very small differences were observed at the exit location by applying the formulation given by Equation 7. Fairly similar results in H_2O and total temperature profiles can be obtained with the EDM compared to the finite-rate chemistry with E-S. Varying the A_{edm} constant has barely any influence on the position of the peak but has a significant influence on the peak value. Adopting a value of 6 for this constant yields peak values similar to experiment and finite-rate chemistry. In terms of the other species profiles increasing the standard setting of $A_{edm} = 4$ does not demonstrate drastic changes. Using a lower value of the model constant ($A_{edm} = 1$) results in a consistent under-prediction of the peak total temperature and related H_2O mole fraction. Both the EDM and the finite-rate chemistry under-predict the penetration depth of hydrogen into the vitiated airflow. The slope of the latter is however in better agreement with the experiments than the former. Overall the best results with EDM are obtained by prescribing $A_{edm} = 6$. The configuration is characterized by the presence of an ignition delay where the combustion process is rate limited and is consequently not captured by the EDM. However, in the profiles discussed above it was shown that the EDM can predict fairly well the combustion occurring near the end of the test sections suggesting a primarily mixing limited reaction zone. The intensity of the combustion required a higher value for the model constant and could be related to the high free-stream temperature. Note that the no-model approach with E-S predicted a certain ignition delay as expected from the rate limited character of the model. As pointed out in section 2, results with EDM required much less computational effort compared to the finite-rate no-model approach. Starting from a converged solution it takes the EDM simulation about 16 h to advance one flow length in time. The same result with finite rate chemistry and the E-S reaction mechanism takes 81 h. One flow length is based on the distance from the entrance of the combustor and the freestream velocity of the vitiated air in Table 1 and is about 0.2 ms. This comparison has been made on 72 CPU cores on the Tinaroo HPC system of the University of Queensland with a CFL setting of 0.5.

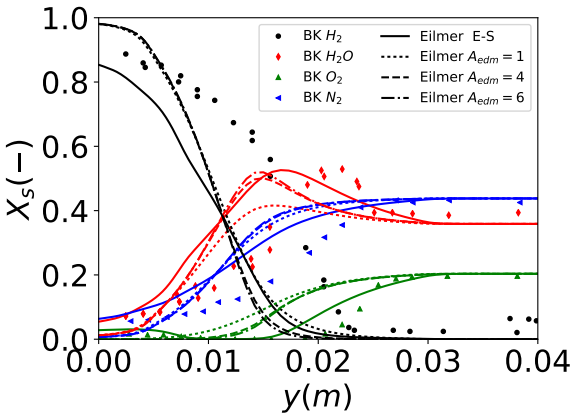

Fig. 2: Predictions of species mole fraction at x=35.6 cm obtained with EDM and the no-model approach compared with experimental values of Burrows and Kurkov.

3.2 Case 2: DLR combustor

Another widely studied test case is the DLR combustor experiment of Waidmann et al. [41] depicted in Figure 4. Just like the Burrows-Kurkov experiment, measurements have been taken in both a pure mixing and a combusting setting. The main geometry is notionally two-dimensional, however the use of porthole injectors on the rear of the strut sets up an inherently three-dimensional flow field. Several two-and three-dimensional RANS studies of this combustor test case can be found in the literature [8, 32–36] where

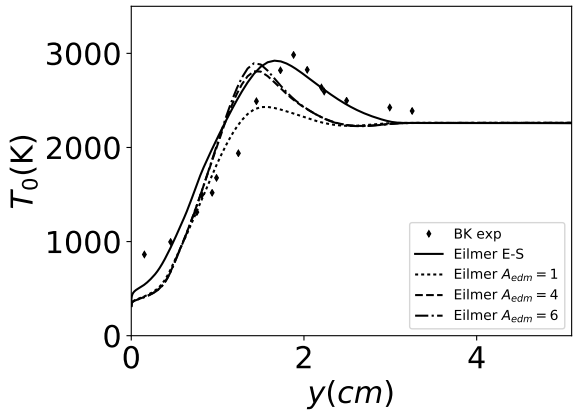

Fig. 3: Predictions of total temperature at x=35.6 cm obtained with EDM and the no-model approach compared with experimental values of Burrows and Kurkov.

each author introduces a TCI model. In spite of the three-dimensionality of the configuration, two-dimenional studies are useful as a proof of concept for modeling techniques. Oevermann [32] and Mura et al. [33] obtained reasonable results in their two dimensional studies. Following this approach, the present work considers the application of EDM on a two-dimensional domain with single slot injector. It is expected that the two-dimensional assumption will introduce a certain degree of error.

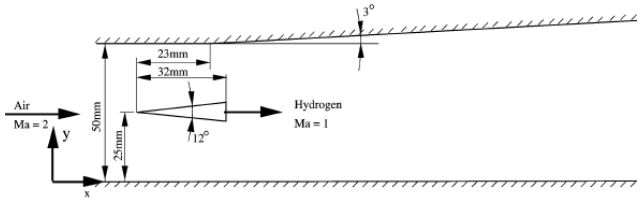

Fig. 4: Schematic of the DLR combustor experiment [32].

3.2.1 Problem Formulation

A structured grid has been generated for the domain shown in Figure 4 containg 117 000 cells. The distance between the supersonic inlet, with conditions given in Table 2, and the start of the strut is taken as 18 mm and the total combustor length as 300 mm. Upper and lower walls are treated as inviscid which is an acceptable choice given the distant location with respect to the reaction zone. The strut walls are defined adiabatic with a maximum first cell wall distance of 5e-6 m ensuring that the first cell is in the visous sublayer. Given the relatively low stream temperatures in the combustor and the location of the reaction zone further downstream of the strut, the heat transfer to the strut walls is expected to be small supporting the adiabatic wall boundary condition setting. Supersonic outflow is assumed. Turbulence quantities are taken similar to Oevermann [32] and Mura et al. [33]: for the free stream inflow $I = 0.3\%$, $\mu_t/\mu = 675$ and for the injector $I = 3.3\%$, $\mu_t/\mu = 63$. Similarly to the Burrows and Kurkov test case, a sensitivity study for combinations of Pr_t and Sc_t was performed with standard EDM settings ($A_{edm} = 4$, no limiting). Based on a comparison with experimental data, fairly similar results were observed with a value of 0.9 or 0.5 for both parameters. The former option is presented in this work.

Table 2: Inflow and injector flow conditions for the DLR combustor experiment.

	inflow	injector
u (m/s)	730.0	1200.0
T (K)	340.0	250.0
p (Pa)	100000.0	100000.0
Y_{H_2} (-)	0.0	1.0
Y_{O_2} (-)	0.232	0.0
Y_{H_2O} (-)	0.032	0.0
Y_{N_2} (-)	0.736	0.0

3.2.2 Results

The DLR combustor test case has proven to be very challenging to predict in a two-dimensional context. Multiple combinations of the different settings were explored and only a limited number of results will be discussed in this paper. Waidmann et al. [41] collected, inter alia, data on axial velocity and temperature respectively at the cross-sections marked with 1,2,3 and 1,2,4 in Figure 5.

In Figures 7 and 8 the axial velocity component is compared to experiments at the first two cross-sections. Two-dimensional numerical predictions by Oevermann [32] obtained with the k-ϵ turbulence model, a combination $Pr_t = Sc_t = 0.7$ and a flamelet TCI model in conjunction with the reaction mechanism of Maas and Warnatz are shown as well. Reducing the model constant A_{edm} to 1 did not show any significant difference in the CFD prediction of Eilmer. At the first location an asymmetric double peak is predicted by the solver with an inverse behavior in the CFD of Oevermann. In comparison with the experimental data both seem to fail in capturing the correct behavior. Simulations using a more advanced description of turbulence [47–49] in a three-dimensional context have shown a much less pronounced asymmetry and the presence of the two recirculation regions behind the strut extending to this location. Eilmer's prediction does show the presence

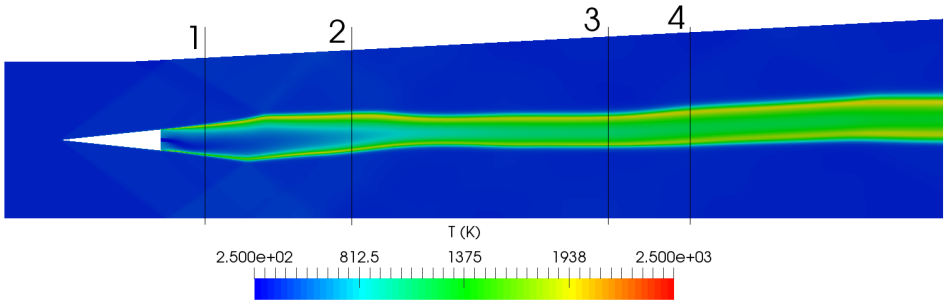

Fig. 5: Temperature contour ($A_{edm} = 4$) with indication of the axial locations used in in the DLR combustor experiment [41] for measurement of velocity (1,2,3) and temperature (1,2,4).

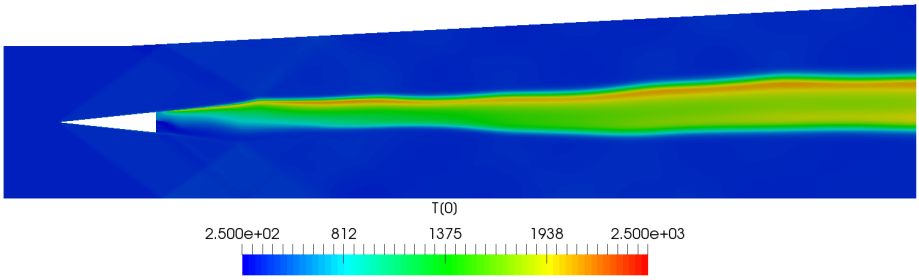

Fig. 6: Temperature contour ($A_{edm} = 4$) of the DLR combustor experiment [41] obtained with the finite-rate limit.

of only the upper recirculation region while Oevermann captures none.

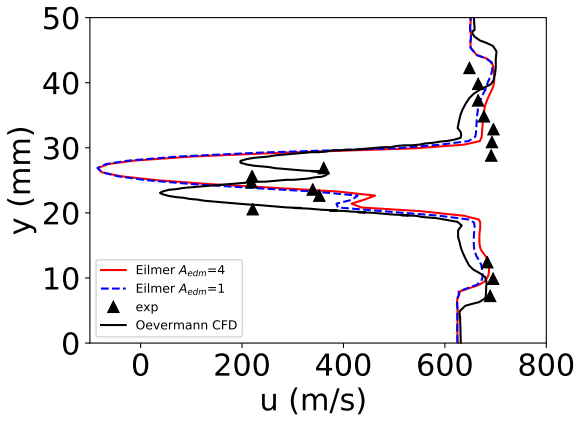

Fig. 7: Effect of the EDM model constant on the velocity profile at cross-section 1 in the DLR combustor.

At the second cross-section, velocity profiles of Eilmer and the reference CFD of Oevermann are similar with a peak location which is not aligned with experimental trend. It must be noted that even the more advanced CFD models [47–49] do not yield a good agreement with this particular set of experimental data which demonstrates the challenging nature of the test case.

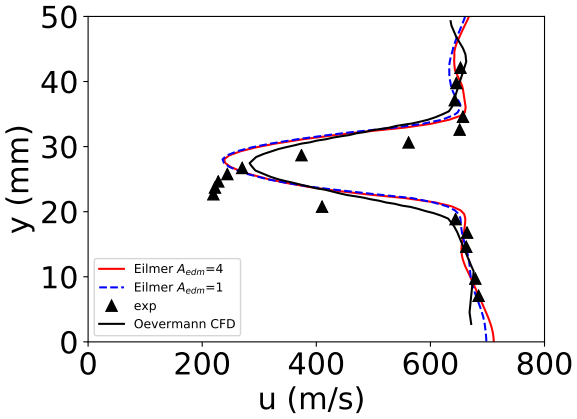

Fig. 8: Effect of the EDM model constant on the velocity profile at cross-section 2 in the DLR combustor.

Figure 9 shows the temperature prediction at the first cross-section while Figure 10 presents the same variable at the fourth cross section. In contradiction to the axial velocity profiles, the results are very sensitive to the value of the EDM constant. More specifically, a value $A_{edm} = 1$ predicts a lower reaction rate and consequently lower peak temperature values. At the first cross-section, the EDM predicts a double peak behavior which is observed experimentally as well. The standard setting ($A_{edm} = 4$) does seem to over-predict the reaction rate compared to Oevermann as well as other finite-rate chemistry results including more detailed reaction mechanisms [47–49]. Reducing the rate of reaction of the EDM model to $A_{edm} = 1$ is perhaps the better choice for the DLR combustor simulations.

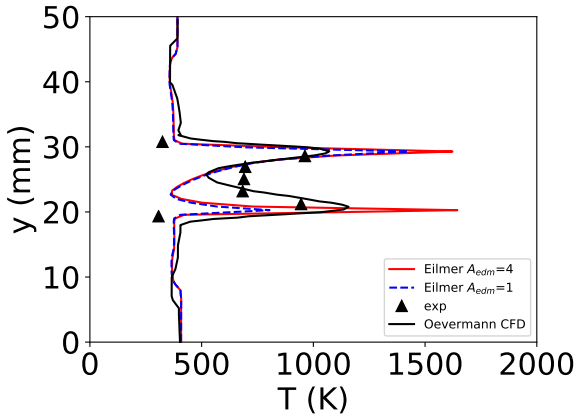

Fig. 9: Effect of the EDM model constant on the temperature profile at cross-section 1 in the DLR combustor.

CFD predictions at the last cross-section, presented in Figure 10, have much less agreement with experimental values as well as with other RANS predictions found in the literature [8, 32–35]. It must be noted that no simulations using the Wilcox k-ω 2006 model on the DLR combustor configuration have been reported. The k-ϵ and the k-ω SST models are used instead. The capability of the k-ω 2006 model in dealing with shear layers has however been demonstrated in the previous test case of Burrows and Kurkov as well as with the coaxial mixing of two jets [12]. From the experimental observations, a single temperature peak should be numerically predicted instead of a double peak. The peak strengths can be mitigated with a lower model constant setting. As shown in the temperature contour (Figure 5), intense burning is observed in the upper and lower mixing layers in the region downstream the strut toward the end of the domain suggesting a lack of heat conduction toward the center. The behavior could be improved by influencing the diffusion process of the species and / or the enthalpy gradient. This relates to the values of Pr_t and Sc_t in the viscous term of the energy and species equations respectively. The path of reducing both constants has been explored without success. Another possible cause related to the same governing equations is the effect of the stress limiter on the eddy viscosity introduced in the latest version of the k-ω 2006 [11] and has to be investigated. Other than the turbulence model, the three-dimensionality of the problem could be an explanation as well for the observed effect in the present work. This statement follows from the fact that in a three-dimensional setting with the k-ϵ turbulence model and the EDM, Dharavath et al. [8], demonstrated a closer agreement with experiments at this last cross-section.

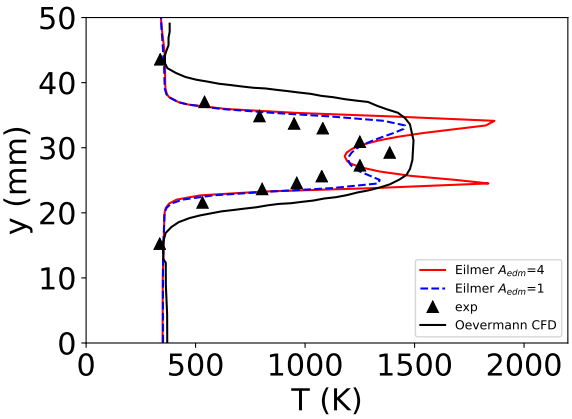

Fig. 10: Effect of the EDM model constant on the velocity profile at cross-section 4 in the DLR combustor.

The effect of activating the global reaction limiting option with Equation 7 has as well been investigated. Simulations were initiated from the converged EDM result without limit as to avoid the need for a source of ignition given the low free-stream temperatures. Profiles of axial velocity did not show significant differences however the temperature profiles did. This can be understood with Figure 6 presenting the resulting temperature contour for the standard setting $A_{edm} = 4$ which can be compared with Figure 5. Applying the reaction rate limit does suppress combustion in the lower recirculation region just downstream of the strut. This in turn results in a single temperature peak and is not in agreement with the experimental data (Figure 9). Further downstream, combustion starts to establish across the wake region and finally near the end of the domain the more intense shear layer combustion is observed, similarly to Figure 5 but more asymmetric. The spreading of the

reaction zone is larger with limit than without. Overall the two-dimensional results applying Equation 7 are in worse agreement with experimental measurements.

The three-dimensional simulation path might be an unavoidable step in order to draw definitive conclusions about the application of EDM for the DLR combustor test case. Even then the suitability of RANS for such a strut injection mixing layer configuration might become questionable.

3.3 Case 3: Lorrain's scramjet

The third test case is a scramjet geometry investigated by Lorrain et al. [42, 50] in the University of Queensland's T4 piston-driven shock tunnel. The scramjet design relies on the concept of radical farming and has been simulated in two-dimensional premixed conditions with CFD++ [51] by Lorrain et al. [42]. Figure 11 shows the semi-free jet configuration at an equivalent flight Mach number of 9.7 and a dynamic pressure of 57.7 kPa at an altitude of 31.9 km. By semi-free jet configuration we mean a configuration where the flow entering the geometry is representative of the flow behind a vehicle forebody shock.

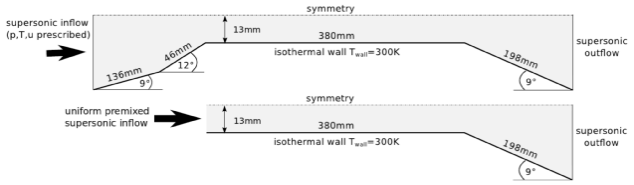

Fig. 11: Schematic of the scramjet geometry of Lorrain [42].

3.3.1 Problem Formulation

The simulations are performed with structured grids in three stages with the first stage consisting of a fuel-off configuration making use of the upper representation of Figure 11. Free stream boundary conditions for this simulation are summarized in Table 3 and turbulence quantities are set to $I = 2\%$ and $\mu_t/\mu = 5$ in accordance with Lorrain's settings while Pr_t is taken as 0.89. In the second stage, the lower representation is considered with hydrogen suppressing any combustion (frozen). The fuel-off inflow profile at the entrance of the combustor is taken as the inlet boundary condition of the frozen (and combusting) test case. To account for the presence of fuel, the pressure profile was altered as $p_{frozen} = p_{fuell-off}/(1 - X_{H_2})$. The frozen result is taken as the initial field for the reacting simulations. The first two stages have already been presented by the same authors [13]. In the combusting condition, Sc_t is set to 0.7. Given the premixed character of the simulation, the product term in Equation 5 is included in the EDM computations. An initial product (H_2O) mass fraction of 0.01 is uniformly specified in the domain. Supersonic outflow is assumed similarly to case 1 and isothermal walls at 300 K.

Table 3: Flow conditions at the inlet of the scramjet geometry for the different simulations [42].

	fuel-off	frozen / reacting
u (m/s)	2830	u(y)
p (Pa)	4100	p(y)
T (K)	370	T(y)
X_{O_2}(-)	0.21	0.157
X_{N_2}(-)	0.79	0.593
X_{H_2}(-)	0.0	0.25

3.3.2 Results

Figure 12 shows the pressure profile along a streamline starting at the entrance of the combustor, 1.5 mm from the lower wall. Lorrain [42] performed finite-rate numerical simulations using the reaction mechanism of Jachimowski [52] with 13 species and 33 reactions. This result will be used as the reference to discuss the performance of the EDM. The test case demonstrated the importance of introducing a limit on the reaction rates predicted by the EDM as the unlimited simulations resulted in unphysically high peak temperatures coupled with an unstart behavior where the shock-induced boundary layer separation bubble at the first shock impingement inside the combustor was continuously growing in the upstream direction. Therefore the EDM curves in Figure 12 are obtained by applying the limit in Equation 7. The pressure profiles show that the use of a lower A_{edm} value results in a better prediction of the ignition delay when compared to the reference CFD. Shock strengths are however underpredicted with a lower value. The standard setting of 4 consistently results in stronger shocks and is not an adequate choice for simulating this configuration. Moreover, ignition occurs much earlier for the standard EDM setting. From observation of the pressure curves a setting of A_{edm} between 1 and 1.5 is advised for the scramjet which is a compromise between accurate prediction of shock position and shock strength. The numerical results confirm the lower limit for the model constant, $A_{edm} = 1$, suggested by Edwards et al. [6]. An important conclusion is that EDM with kinetic limit can predict the ignition delay in a scramjet engine relying on the concept of radical farming which is a phenomenon present for instance in the Rectangular-To-Elliptic Shape Transition (REST) scramjet configuration used in the HIFiRE program [53].

Figure 13 shows the effect of the limiting choice on EDM along the same streamline as in previous discussion. The

threshold temperature of 900 K used by Edwards et al. [6] is compared to the no-model limit with coefficients obtained from [7, 8] (Equation 7). In this comparison, the lower limit of the model constant is applied. The streamline pressure with a threshold temperature (T_{lim}) predicts a much stronger shock induced boundary layer separation bubble near the entrance of the combustor around x = 3.69 cm. With the same settings, ignition occurs earlier compared to the reference CFD and the no-model limit. Except for the first shock reflection, adopting $T_{lim} = 900K$, results in a similar behavior as in Figure 12 for the case $A_{edm} = 1.5$. In order to avoid the separation bubble size over-prediction in this scramjet it is preferable to combine the no-model limit with a setting of A_{edm}. Regarding the use of the product term and the constant B_{edm}, as steady state results are presently targeted, no effect was observed on the final result.

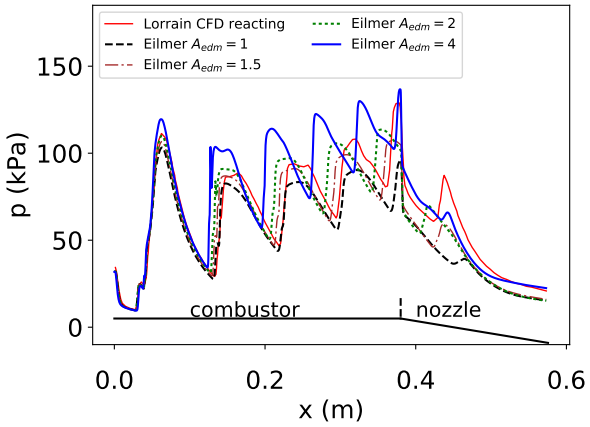

Fig. 12: Pressure along a streamline, originating 1.5 mm from the wall at the combustor entrance, as predicted with several values of the model constant A_{edm} for Lorrain's scramjet.

4. Discussion and Conclusions

In this work the application of the Eddy Dissipation Model (EDM) for scramjet design purposes has been explored by simulating three hydrogen-fueled scramjet configurations. Turbulence is described by Wilcox' k-ω 2006 model. The test cases are representative for different types of scramjet combustors. An overall good agreement was observed for the Burrows-Kurkov test case in comparison with experimental data and finite-rate, no-model chemistry at the exit of the domain. The DLR combustor simulations have shown some discrepancies with a decreasing experimental agreement toward the end of the test section. The intrinsic three-dimensionality of the configuration could be the main

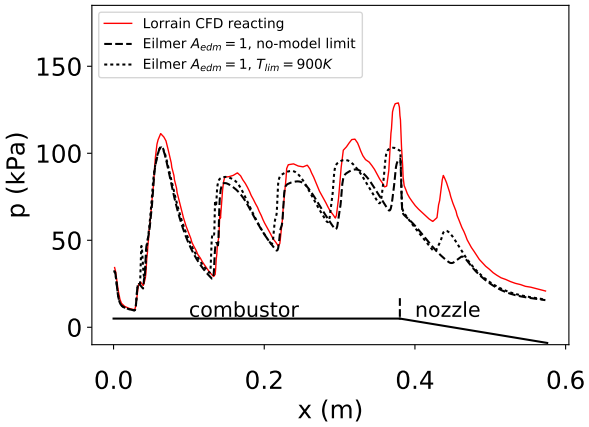

Fig. 13: Effect of the approaches on limiting the reaction rates predicted by EDM for Lorrain's scramjet.

reason for this and has to be explored. The third scramjet test case, the experiment of Lorrain, has demonstrated the effect and importance of applying a limit on the reaction rate predicted by the EDM. In terms of the A_{edm} constant setting a value of 6 was more appropriate for the experiment of Burrows-Kurkov while the DLR combustor and Lorrain's scramjet suggested a much lower value of 1. Some thoughts are now given on the possible reasons behind this observation. In spite of both the Burrows-Kurkov and the DLR combustor showing the presence of mixing layers, the EDM constant requirements yielding the best agreement with experimental values are very different. The higher freestream temperature in the experiment of Burrows-Kurkov compared to DLR could be the reason for a stronger combustion near the end of the configuration which required an increase in fuel consumption through A_{edm} to match the experimental mean peak temperature. Nevertheless, the shear layer is very different from the DLR combustor as fuel and vitiated airstream are only separated by a small step. On the other hand, the scramjet of Lorrain was best predicted with a similar setting to the DLR combustor having no physical features in common except perhaps the presence of multiple shock reflections. The latter is not a key feature in the experiment of Burrows and Kurkov. Based on the current observations, one could argue that lower values for A_{edm} are required in the presence of multiple shock reflections but this statement should be considered speculative. Keeping a low value of the model constant in Lorrain's scramjet simulation was needed in order to keep the fuel reaction rate low and avoid overprediction of combustion near the physical walls of the geometry coupled with unphysically high mean temperatures. The same effect was mitigated in the shear

layers of the DLR combustor by a similar EDM setting. The computational advantage of the EDM was demonstrated by comparison with finite-rate, no-model chemistry in the Burrows-Kurkov experiment. In this test, the targeted steady-state answer was obtained four times faster with EDM compared to the seven species, eight reactions nechanism of Evans and Schexnayder. The present exploration of the EDM demonstrates the need for careful case-dependent calibration with the capability to result in predictions with a reasonable degree of accuracy at a reduced computational cost. This characteristic makes the CFD model potentially useful for scramjet design purposes. Further investigations are required in order to obtain more general conclusions about the method and enable the formulation of guidelines on its optimal use.

Acknowledgements
The authors would like to express their gratitude to Dr. Peter Jacobs from the University of Queensland for the many discussions and suggestions during the realization of this work. This work has been realized with the support of the J.M. Lessells Scholarship of the Royal Society of Edinburgh and the Mac Robertson Scholarship jointly provided by the University of Strathclyde and the University of Glasgow. Grateful acknowledgement is hereby made to the donors of the said funds.

References

[1] D Preller and MK Smart. Scramjets for reusable launch of small satellites. In *20th AIAA International Space Planes and Hypersonic Systems and Technologies Conference*, page 3586, 2015.

[2] SO Forbes-Spyratos, MP Kearney, MK Smart, and IH Jahn. Trajectory design of a rocket-scramjet-rocket multi-stage launch system. In *21st AIAA International Space Planes and Hypersonics Technologies Conference*, page 2107, 2017.

[3] RA Baurle. Modeling of high speed reacting flows: established practices and future challenges. *AIAA paper*, 267:2004, 2004.

[4] NJ Georgiadis, DA Yoder, MA Vyas, and WA Engblom. Status of turbulence modeling for hypersonic propulsion flowpaths. *Theoretical and Computational Fluid Dynamics*, 28(3):295–318, 2014.

[5] BF Magnussen and BH Hjertager. On mathematical modeling of turbulent combustion with special emphasis on soot formation and combustion. In *Symposium (international) on Combustion*, volume 16, pages 719–729. Elsevier, 1977.

[6] Jack R Edwards and Jesse A Fulton. Development of a RANS and LES/RANS flow solver for high-speed engine flowpath simulations. In *20th AIAA International Space Planes and Hypersonic Systems and Technologies Conference*, page 3570, 2015.

[7] MSR Chandra Murty and D Chakraborty. Numerical simulation of angular injection of hydrogen fuel in scramjet combustor. *Proceedings of the Institution of Mechanical Engineers, Part G: Journal of Aerospace Engineering*, 226(7):861–872, 2012.

[8] M Dharavath, P Manna, and D Chakraborty. Thermochemical exploration of hydrogen combustion in generic scramjet combustor. *Aerospace Science and Technology*, 24(1):264–274, 2013.

[9] RJ Gollan and PA Jacobs. About the formulation, verification and validation of the hypersonic flow solver Eilmer. *International Journal for Numerical Methods in Fluids*, 73(1):19–57, 2013.

[10] PA Jacobs and RJ Gollan. Implementation of a compressible-flow simulation code in the D programming language. In *Applied Mechanics and Materials*, volume 846, pages 54–60. Trans Tech Publ, 2016.

[11] DC Wilcox. Formulation of the k-ω turbulence model revisited. *AIAA journal*, 46(11):2823–2838, 2008.

[12] WYK Chan, PA Jacobs, and DJ Mee. Suitability of the k–ω turbulence model for scramjet flowfield simulations. *International Journal for Numerical Methods in Fluids*, 70(4):493–514, 2012.

[13] JJOE Hoste, V Casseau, M Fossati, IJ Taylor, and RJ Gollan. Numerical modeling and simulation of supersonic flows in propulsion systems by open-source solvers. In *21st AIAA International Space Planes and Hypersonics Technologies Conference*, page 2411, 2017.

[14] MN Macrossan. The equilibrium flux method for the calculation of flows with non-equilibrium chemical reactions. *Journal of Computational Physics*, 80(1):204–231, 1989.

[15] M.S. Liou. Ten years in the making - AUSM-family. *AIAA Paper*, pages 2001–2521, 2001.

[16] T Poinsot and D Veynante. *Theoretical and Numerical Combustion, third edition*. RT Edwards, Inc., 2012.

[17] JS Evans and CJ Schexnayder. Influence of chemical kinetics and unmixedness on burning in supersonic hydrogen flames. *AIAA journal*, 18(2):188–193, 1980.

[18] HB Ebrahimi. CFD validation for scramjet combustor and nozzle flows, part i. *AIAA Paper*, 1840:1993, 1993.

[19] B Parent and JP Sislian. Validation of the wilcox k-omega model for flows characteristic to hypersonic air-breathing propulsion. *AIAA journal*, 42(2):261–270, 2004.

[20] WA Engblom, FC Frate, and Nelson CC. Progress in validation of Wind-US for ramjet/scramjet combustion. In *43rd AIAA Aerospace Sciences Meeting and Exhibit*, Reno, Nevada, January 2005.

[21] V Bhagwandin, W Engblom, and N Georgiadis. Numerical simulation of a hydrogen-fueled dual-mode scramjet engine using Wind-US. In *45th AIAA/ASME/SAE/ASEE Joint Propulsion Conference & Exhibit*, page 5382, 2009.

[22] W Huang, Z Wang, S Li, and W Liu. Influences of h 2 o mass fraction and chemical kinetics mechanism on the turbulent diffusion combustion of h 2–o 2 in supersonic flows. *Acta Astronautica*, 76:51–59, 2012.

[23] Z Gao, C Jiang, S Pan, and CH Lee. Combustion heat-release effects on supersonic compressible turbulent boundary layers. *AIAA Journal*, 53(7):1949–1968, 2015.

[24] CG Rodriguez and AD Cutler. Numerical analysis of the scholar supersonic combustor. 2003.

[25] JP Drummond, SD Glenn, and AD Cutler. Chapter 6: fuel–air mixing and combustion in scramjets. *Technologies for Propelled Hypersonic Flight, NATO-RTO-AVT, National Technical Information Service, Virginia, USA*, 2006.

[26] T Mitani and T Kouchi. Flame structures and combustion efficiency computed for a mach 6 scramjet engine. *Combustion and Flame*, 142(3):187–196, 2005.

[27] J-Y Choi, F Ma, and V Yang. Combustion oscillations in a scramjet engine combustor with transverse fuel injection. *Proceedings of the Combustion Institute*, 30(2):2851–2858, 2005.

[28] J. Steelant, A. Mack, K. Hannemann, and A.D. Gardner. Comparison of supersonic combustion tests with shock tunnels, flight and CFD. In *42nd AIAA/ASME/SAE/ASEE Joint Propulsion Conference and Exhibit*, Sacramento, California, July 2006.

[29] S. Karl, K. Hannemann, A. Mack, and J. Steelant. CFD analysis of the HyShot II scramjet experiments in the HEG shock tunnel. In *15th AIAA International Space Planes and Hypersonic Systems and Technologies Conference*, page 2548, 2008.

[30] PG Keistler, RL Gaffney, X Xiao, and HA Hassan. Turbulence modeling for scramjet applications. *AIAA paper*, 5382:2005, 2005.

[31] MSR Chandra Murty, D Chakraborty, and RD Mishal. Numerical simulation of supersonic combustion with parallel injection of hydrogen fuel. *Defence Science Journal*, 60(5), 2010.

[32] M Oevermann. Numerical investigation of turbulent hydrogen combustion in a scramjet using flamelet modeling. *Aerospace science and technology*, 4(7):463–480, 2000.

[33] A Mura and JF Izard. Numerical simulation of supersonic nonpremixed turbulent combustion in a scramjet combustor model. *Journal of Propulsion and Power*, 26(4):858–868, 2010.

[34] Z Gao, J Wang, C Jiang, and C Lee. Application and theoretical analysis of the flamelet model for supersonic turbulent combustion flows in the scramjet engine. *Combustion Theory and Modelling*, 18(6):652–691, 2014.

[35] L Hou, D Niu, and Z Ren. Partially premixed flamelet modeling in a hydrogen-fueled supersonic combustor. *International Journal of Hydrogen Energy*, 39(17):9497–9504, 2014.

[36] OR Kummitha. Numerical analysis of hydrogen fuel scramjet combustor with turbulence development inserts and with different turbulence models. *International Journal of Hydrogen Energy*, 42(9):6360–6368, 2017.

[37] V. Terrapon, F. Ham, R. Pecnik, and H. Pitsch. A flamelet-based model for supersonic combustion. *Annual research briefs*, pages 47–58, 2009.

[38] M Chapuis, E Fedina, Christer Fureby, Klaus Hannemann, Sebastian Karl, and J Martinez Schramm. A computational study of the HyShot II combustor performance. *Proceedings of the Combustion Institute*, 34(2):2101–2109, 2013.

[39] B Sekar and HS Mukunda. A computational study of direct simulation of high speed mixing layers without and with chemical heat release. In *Symposium (International) on Combustion*, volume 23, pages 707–713. Elsevier, 1991.

[40] MC Burrows and AP Kurkov. An analytical and experimental study of supersonic combustion of hydrogen in vitiated air stream. *AIAA Journal*, 11(9):1217–1218, 1973.

[41] W Waidmann, F Alff, U Brummund, M Böhm, W Clauss, and M Oschwald. Experimental investigation of the combustion process in a supersonic combustion ramjet (scramjet). *DGLR Jahrbuch*, pages 629–638, 1994.

[42] P Lorrain, B Capra, S Brieschecnk, and R Boyce. A detailed investigation of nominally 2-D radical farming scramjet combustion. In *18th AIAA/3AF International Space Planes and Hypersonic Systems and Technologies Conference*, page 5812, 2012.

[43] F.R. Menter. Two-equation eddy-viscosity turbulence models for engineering applications. *AIAA journal*, 32(8):1598–1605, 1994.

[44] KW Brinckman, WH Calhoon, and SM Dash. Scalar fluctuation modeling for high-speed aeropropulsive flows. *Aiaa Journal*, 45(5):1036–1046, 2007.

[45] X Xiao, HA Hassan, and RA Baurle. Modeling scramjet flows with variable turbulent Prandtl and Schmidt numbers. *AIAA journal*, 45(6):1415–1423, 2007.

[46] JR Edwards, JA Boles, and RA Baurle. Large-eddy/Reynolds-averaged Navier–Stokes simulation of a supersonic reacting wall jet. *Combustion and Flame*, 159(3):1127–1138, 2012.

[47] F Génin and S Menon. Simulation of turbulent mixing behind a strut injector in supersonic flow. *AIAA journal*, 48(3):526, 2010.

[48] AS Potturi and JR Edwards. Hybrid Large-Eddy/Reynolds-averaged Navier–Stokes simulations of flow through a model scramjet. *AIAA journal*, 2014.

[49] C Fureby, E Fedina, and J Tegnér. A computational study of supersonic combustion behind a wedge-shaped flameholder. *Shock waves*, 24(1):41–50, 2014.

[50] P Lorrain, S Brieschenk, and R Boyce. Experimental investigation of inlet-injection radical-farming scramjet combustion. In *XXI International Symposium on Air Breathing Engines (ISABE 2013)*, volume 1, pages 1–9. Curran Associates, 2013.

[51] U Goldberg, O Peroomian, S Chakravarthy, and B Sekar. Validation of CFD++ code capability for supersonic combustor flowfields. *AIAA paper*, 3271, 1997.

[52] CJ Jachimowski. An analysis of combustion studies in shock expansion tunnels and reflected shock tunnels. 1992.

[53] MK Smart and MV Suraweera. HIFiRE 7-development of a 3-D scramjet for flight testing. *AIAA Paper*, 7259:2009, 2009.